processes

MDPI

Article

Comprehensive Penetration Evaluation Method in Collisions between a Supply Ship and a Semi-Submersible Platform

Yuan Xiao [1], Zhi Yao [2] and Xu Zhang [2,*]

[1] CIMC Raffles Offshore Ltd., Yantai 264670, China; yuanxiao@cimc-raffles.com
[2] School of Ocean Engineering and Technology, Sun Yat-sen University, Zhuhai 519082, China; yaozh23@mail2.sysu.edu.cn
* Correspondence: zhangx798@mail.sysu.edu.cn

Abstract: Collisions between ships and offshore platforms frequently occur, with severe consequences. Predicting the collision depth under different conditions is very important to evaluate the severity of the consequences. Considering the time-consuming numerical simulation problem and the accuracy problems of existing approximation algorithms, this paper proposes a comprehensive approach to estimating penetration depths by obtaining two collision coefficients for specific collision structures based on the partial results of numerical simulations and simplified theoretical analysis. In this study, the collision process between a supply ship with a transverse framing stern and an offshore semi-platform was first numerically simulated based on the explicit dynamic method. The changes in ship velocity, impact force, and energy conversion before and after the collision processes were obtained through numerical simulations of the collisions with different speeds and angles. Then, by combining the external dynamics and numerical results, the analytical results of dissipated energy under other collision conditions were obtained using a simulated restitution coefficient. For the following internal dynamics analysis, according to the failure modes of specific structural components in different regions, an appropriate structural energy absorption formula was combined to obtain the relationship between the penetrations and energy absorption in a particular collision area. According to the friction energy ratio derived by the simulation, the penetration depths in the offshore platform were calculated. The results showed that the deviations between the proposed method and direct simulation results were less than 15% in the cases of a medium- to high-energy collision. It can be concluded that the restitution coefficient and friction energy ratio in different collision conditions can be approximately determined for a specific collision system by typical numerical simulations, thus quickly calculating the penetration depths of other conditions.

Keywords: ship–platform collision; external dynamics; internal dynamics; penetration depth; energy conversion

Citation: Xiao, Y.; Yao, Z.; Zhang, X. Comprehensive Penetration Evaluation Method in Collisions between a Supply Ship and a Semi-Submersible Platform. *Processes* **2022**, *10*, 1212. https://doi.org/10.3390/pr10061212

Academic Editors: Krzysztof Talaśka, Szymon Wojciechowski and Antoine Ferreira

Received: 1 May 2022
Accepted: 14 June 2022
Published: 17 June 2022

1. Introduction

The offshore industry occupies an essential position in global economic development, offering significant freight volumes of oil and gas [1]. During the lifetime of an offshore platform, supply ships are used to transport personnel and materials for gas and oil offshore platforms. A severe ocean environment and increasingly active offshore platform services expose ships and platforms to the risk of collisions, with potentially catastrophic consequences of oil and gas leakage and severe human life and economic losses [2]. Studies have shown that the impact of collisions on offshore structures is significantly higher than other factors such as fires, engine problems, and hijackings [3,4]. It is essential to assess the consequences of collisions, of which the penetration depth of impact is a crucial indicator. Fast and reliable prediction of the penetration depth of collisions under different conditions could help identify the hazardous situations in replenishment operations and help minimize the collision risk.

A theoretical approach to predicting ship collisions includes three steps. First, analyzing a ship collision scenario for a given area, which involves many complex factors. Most of the current predictions for ship collision scenarios are based on accident records, and the main methods are fault tree analysis (FTA) and event tree analysis (ETA) [5–7]. Ramos [8] combined FTA and Bayesian networks for hybrid causal logic analysis. For further consideration of traffic complexity in practice, Zhang [9] proposed a method to predict collision probabilities and generate scenarios for ship damage stability assessments using an automatic identification system (AIS).

External dynamics analysis and internal dynamics analysis are then conducted. The former analysis of a ship collision aims to predict the initial kinetic energy loss absorbed due to the plastic deformation and rupture of the ship structure by considering the rigid body motion of the ship and the effects of water. The subsequent internal dynamics analysis, on the other hand, is intended to estimate the structural damage sustained by the ship.

For the external dynamics methods, Minorsky [10] proposed an external dynamics analysis method to calculate the lost kinetic energy of ship collision concerning the initial kinetic energy, which was applied to right-angle and central collisions. To extend the application, Petersen [11] carried out the first time-domain simulation of a two-dimensional oblique collision. Based on this, Petersen and Zhang [12] established an analytical method for the energy loss and impact impulse of an arbitrary ship in a horizontal plane collision, which applies to different collision angles and positions. In this method, the collision object was assumed to be a rigid body and the effects of friction during the instantaneous collision and the additional hydrodynamic forces when the ship accelerated were considered. Their results were cross-validated with the work of Petersen [11]. Brown [13] developed a simplified collision model (SIMCOL) in the time domain that was combined with a Monte Carlo method to investigate the effect of random variables such as collision speed, angle, displacement, and ship type on the collision damage degree, confirming that the method of Petersen and Zhang [12] was accurate. In addition, Tabri [14] proposed a theoretical model to predict the consequences of ship collisions in which the swaying effect of a ship with fully loaded ballast tanks and the elastic buckling of the hull beam. Liu [15] presented a collision matrix for the first time to define the role of translational and rotational motion during an impact. After the comparison with other classical impact mechanics models, it was found that the method had less conservative results and provided detailed information on the lateral and vertical energy dissipation at the contact surface. The method unifies the existing normal, planar space, and multi-planar space approaches.

In the studies based on internal dynamics to analyze collision damage to ship structures, empirical formulas, simplified methods [12,16], and finite element simulations [17–19] have found applications. Haris [20], Sun [21], and Liu [22,23] studied the damage, deformation, and failure of ship components in collisions using simplified analysis approaches. They proposed a corresponding computational model by comparing the model tests with simplified analysis methods. Liu [24] compared the differences between the decoupled and coupled methods in predicting deformation and the rupture of ship structures. The external dynamics in the decoupled method was directly applied in Petersen and Zhang [12], while the internal dynamics was performed using the LS-Dyna finite element solver. The numerical model proposed by Pill [25] was used in the coupled method. Liu [26] carried out numerical simulations in ABAQUS on the process of a falling container impacting the deck of an offshore platform and observed significant plastic deformation. They also proposed two simple methods to extend the failure strain to a wider triaxiality range.

From the above research on the evaluation of ship collision damage, experimental studies are the most direct and accurate way of investigating ship collision damage, and can provide validation for other methods. However, model tests are expensive and are affected by scale effects. Both empirical formulas and simplified methods have high calculation efficiency, but obtaining the desired accuracy is difficult, especially for complex practical engineering problems. With the development of computer technology, finite element numerical modeling has gradually become a popular method for studying collision

problems, but the numerical simulation of many collision conditions can be time-consuming. For the simulations, certain problems may exist in failure definition and parameter setting.

This paper introduces a method of combining simplified analysis and numerical simulation. Meanwhile, since supply ship–offshore platform collision has a high frequency of occurrence and severe consequences, there are still few suitable methods for estimating its collision penetration. This study focused on the specific collision process of a supply ship stern and an offshore platform to predict the penetration depth of the collision under multiple conditions, and ultimately to achieve significant risk avoidance. The specific ideas of the proposed method are as follows. According to the simulation results, two key coefficients in different collision scenarios vary slightly. Therefore, with the results of typical numerical simulations, the two coefficients in different collision scenarios could be evaluated and used in simplified analysis based on the external dynamics and internal dynamics. Finally, the corresponding collision depths could be derived. The proposed combining method provides an efficient way of estimating collision penetration depths for multiple collision conditions in practical engineering, which is helpful for preliminary structural design in offshore structures in various possible collision risks.

2. Numerical Analysis of Collision Process

The collided ship selected was a typical transom stern supply ship with the displacement of 5000 t. The collided platform was an ocean support platform with the displacement of 33,500 t. The collision response characteristics under different collision conditions were explored through the numerical simulation of the collision process.

2.1. Collision Conditions

There are three typical types of ship–platform collision: bow collision, stern collision, and side collision. DNV [27] regulations point out that in replenishing offshore platforms by supply ships, the probability of stern collisions account for 70%, side collisions for 20%, and the possibility of bow collision is minimal. According to the structural characteristics of the supply ship stern studied in this paper, the stern is provided with a large cargo deck. Its berthing operation is usually at the stern or side to the target platform. Therefore, the ship stern collision was selected as the collision case. In the collision accident scene specified by DNV, the mass of the collision ship was 5000 t and the collision speed was 2 m/s. Considering the rapid development of ship power systems, collision speeds of 2 m/s, 4 m/s, and 6 m/s were considered. Figure 1 shows the collision condition of the supply ship and the platform in different directions.

Figure 2 shows the corresponding draught at the strong frame and the impact between the strong frames. The angle and height of impact collaboratively determine the location of the supply ship hitting the column. For the convenience of the following description, various collision conditions are summarized in Table 1, where the collision conditions are noted for an explanation.

Table 1. The introduction of the collision condition.

Number	Abbreviations	Explanation
S-SP-6X-H1	S-SP1	Impact the strong frame of column C of the platform 6 m/s
S-SP-2X-H1	S-SP2	Impact the strong frame of column C of the platform 2 m/s
S-SP-4X-H1	S-SP3	Impact the strong frame of column C of the platform 4 m/s
S-SP-6X-H2	S-SP4	Impact between the strong frame of column C on the platform 6 m/s
S-SP-6Y-H1	S-SP5	Impact the strong frame of column C of the platform 6 m/s
S-SP-6XY-H1	S-SP6	Impact the strong frame of column C of the platform 6 m/s

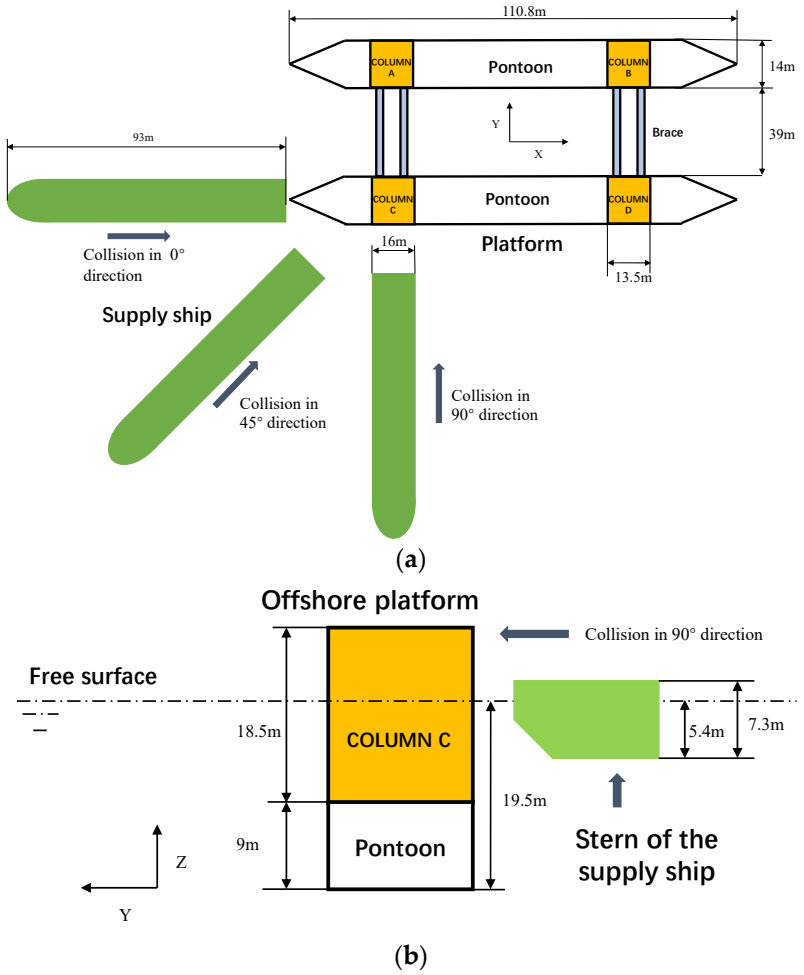

Figure 1. The collision sketch between the supply ship and support platform. (**a**) Top view of collision of offshore platform and ship in different directions. (**b**) Side view of the collision in 90° direction in the H2 condition.

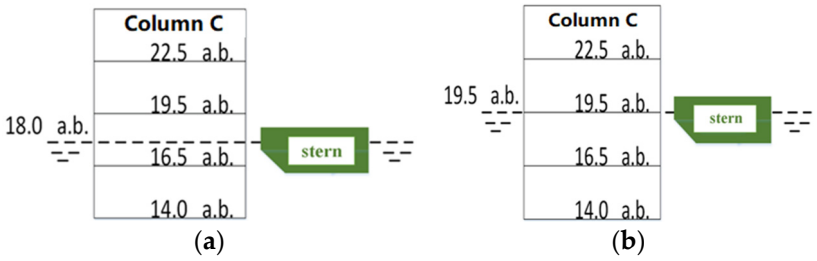

Figure 2. The collision height of the supply ship and support platform. (**a**) Striking the strong frame (H1); (**b**) Impact between strong frames (H2). a.b. is the abbreviation of above baseline, which means the height from the baseline. H1 means the collision height equal to 18.0 m, while H2 means the collision height is equal to 19.5 m. Frame refers to the frame structure composed of the stiffened plate and circumferential truss in the column of a semi-submersible platform.

2.2. Numerical Model Establishment

Generally, in the process of collision between a ship and an offshore platform, large-scale elastic–plastic deformation will be generated in the collision area of the platform to absorb most of the energy, while the deformation is relatively small for the collided ships. This paper was based on the DNV [28] ductile design criterion, which regards the collided ship as a rigid body and neglects the structural deformation of the ship. This will make the obtained analysis results slightly larger than the actual structural damage of the offshore

platform, achieving a conservative damage assessment. Therefore, in the numerical model, the supply ship was set as a rigid body, and the structure of the supply ship was simplified with only the hull and main cabin. The principal dimensions of the supply ship are shown in Table 2.

Table 2. The principle dimensions of the supply ship.

Length (m)	Beam (m)	Depth (m)	Design Draft (m)	Full Load Displacement (t)
93.0	16.0	7.3	5.4	5000

For small-sized stiffeners and longitudinal and transverse timbers, according to the experimental results of Jeom [29] based on the axial crush model of square pipes, the cross-sectional area of the aggregate was spread out on the whole plate connected to it. The method of the equivalent plate thickness [29] is as follows:

$$t_{eq} = t + k\frac{A_s}{b} \quad (1)$$

where t_{eq} is the equivalent plate thickness, while t is the original plate thickness. A_s represents the cross-section area of the aggregate, and b is considered to be the interval of the aggregate, and k is the 'influence factor' of the aggregate on the overall stiffness, which is used to measure the activity of the aggregate. The general value of k was defined as 1.0.

The lower floating body of the platform adopted a simple box-shaped structure, and the upper hull was also a regular box-shaped structure. The lower part of the upper hull had four upright columns of equal height. The columns were mainly composed of the outer plate, watertight platform, non-watertight platform, watertight channel enclosure, watertight cabin, vertical stiffener, and horizontal stiffener. For the structure in the collision area, because obvious elastic–plastic deformation and even serious damage will occur in the process of collision, in the analysis process, a tiny size of the element may appear. The integral step size can be greatly reduced, which will affect the efficiency and accuracy of the whole simulation. Therefore, small characteristic components such as a small bracket plate, narrow flange plate, rib plate with a small opening, and welding seam of the impacted column need to be simplified appropriately. The same simplification was used for the components far from the collision zone. The main parameters of the platform and the supply ship are shown in Table 3.

Table 3. The main structural parameters of the support platform and the supply ship.

Name of Structure		Parameter	Value
Offshore platform	Pontoon	Length	110.3 m
		Width	14.0 m
		Height	9.0 m
		Spacing	39.0 m
	Column	Length	13.5 m
		Width	14.0 m
		Height	18.5 m
		Longitudinal spacing	52.5 m
		Horizontal spacing	53.0 m
	Platform	Draft	18.5 m, 19.5 m
		Displacement	33,500 t
Supply ship		Length	93.0 m
		Width	16.0 m
		Depth	7.3 m
		Draft	5.4 m
		Displacement	5000 t

According to the conclusion drawn by Korgesaar [30], the results were relatively reliable when the ratio of the mesh size to structure thickness in the collision region was 2–20. Therefore, in this paper, a larger mesh size of 0.1 m was adopted in the non-collision zone in both the ship and the platform, and the mesh size of the collision zone was refined to 0.03 m. Figure 3 shows the internal structure of the rammed column, and Figure 4 is a partial enlarged view of the detailed area of the supply ship.

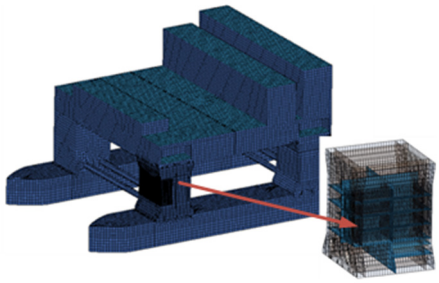

Figure 3. The internal structure of the collided column.

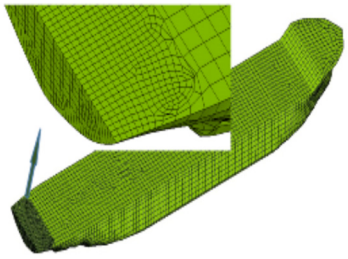

Figure 4. The gridding of ships.

2.3. Main Parameters in Numerical Simulation

In the case of collision between the ship and the offshore platform, the column structure of the platform subjected to collision will bear a huge impact load within a short time (about 2 s). The structural material in the impact area quickly changes from the elastic deformation stage to the plastic flow stage, and then the response of the collapse, fold, penetration depth, and fracture is affected. Jones [31] demonstrated through experiments that the plastic properties of marine steel were highly sensitive to strain rate and its yield stress. The tensile strength limit rose with the increase in the strain rate, while its ultimate fracture strain decreased with the increase in the strain rate. Therefore, the elastic–plastic model should be considered in the selection of materials, and the effect of the material strain rate should be taken into account. In this paper, the widely used Cowper–Symonds strain rate constitutive equation is applicable to the theoretical analysis and numerical calculation. It had a good fitting with the experiment data, and is shown as follows [32]:

$$\dot{\varepsilon} = D\left(\frac{\sigma_{yd}}{\sigma_{ys}} - 1.0\right)^{p} \sigma_{yd} \geq \sigma_{ys} \tag{2}$$

In the above formula, σ_{yd} and σ_{ys} represent the plastic strain rate for epsilon $\dot{\varepsilon}$, dynamic yield stress, and quasi-static yield stress, respectively. Both D and p are constant. Offshore platform material is low carbon steel, taking D as 40.4, and p as 5.

The relationship between the ultimate fracture strain and strain rate of the structural materials is commonly expressed as follows [32]:

$$\frac{\varepsilon_{rd}}{\varepsilon_{rs}} = \left(1.0 + \left(\frac{\dot{\varepsilon}}{D}\right)^{\frac{1}{p}}\right)^{-1} \tag{3}$$

where ε_{rd} is the dynamic fracture strain, and ε_{rs} is the static fracture strain. Koy et al. [33] proposed a practical method to define the dynamic fracture strain and derived an empirical formula as a function of collision velocity to determine the strain rate, thereby determining the dynamic fracture strain. The empirical formula of strain rate [33] is shown as follows:

$$\dot{\varepsilon} = 2.97\nu - 0.686 \tag{4}$$

where ν is the Poisson's ratio.

In the process of high-energy collision, fracture failure often occurs to structural components. In the process of finite element simulation, the failure strain value of the material is usually defined to accurately simulate this phenomenon. For the determination of material failure strain in this paper, the relationship curve between the failure strain and grid size of mild steel was referred [34]. As shown in Figure 5, the corresponding failure strain value was determined according to the element size of 30 mm. Tables 4 and 5 show the specific parameters of the two kinds of materials in this paper.

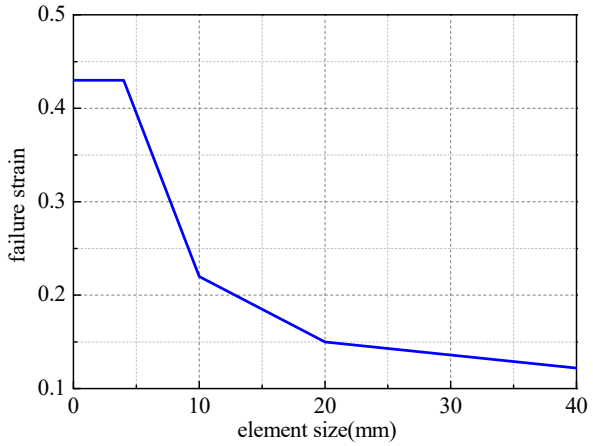

Figure 5. The relationship between the element size and failure strain.

Table 4. The rigid body material parameters.

Density ρ (kg/m^3)	Elastic Modulus E (N/m^2)	Poisson's Ratio ν
According to the COG and added mass	2.1×10^{11}	0.3

Table 5. The elastoplastic material parameters.

Density ρ (kg/m^3)	Elastic Modulus E (N/m^2)	Poisson's Ratio ν
According to the COG and added mass	2.1×10^{11}	0.3
Yield Stress σ_y (Pa)	**Tangent Modulus E_h (Pa)**	**Parameter D (s^{-1})**
3.55×10^8	1.46×10^9	40.4
Parameter P	**Failure Strain ε_f**	
5.0	0.136	

In the process of collision between the ship and the offshore platform, since the collision time is really short, the fluid around the structure will move along with the structure at the moment of impact, which is equivalent to increasing the mass of the structure so that the inertial effect of the structure will also be increased. In the numerical simulation, two methods can be used to deal with the fluid around the structure, namely, the fluid–solid coupling method and added mass method. The added mass method was first proposed by Minorsky [10], and the fixed value 0.4 was used as the added mass coefficient of the

collided ship with swaying motion. In this paper, the attached water quality was analyzed by the added mass method, and the added mass coefficient is shown in Table 6 [10,12]. The added mass coefficient under each collision condition is shown in Table 7.

Table 6. The added mass coefficients of the supply ships and the platforms.

Motion	Surge	Sway	Heave	Roll	Pitch	Yaw
Ship	0.1	0.4	1	0.1	1	0.21
Platform	0.1	0.2	1	1.0	1	0.21

Table 7. The added mass coefficient under each collision condition.

Collision Condition	Ship	Platform
S-SP1	0.1	0.1
S-SP2	0.1	0.1
S-SP3	0.1	0.1
S-SP4	0.1	0.1
S-SP5	0.4	0.2
S-SP6	0.25	0.15

2.4. Numerical Simulation Results

In this section, some of the obtained numerical simulation results were analyzed to gain the key coefficients used in the theoretical analysis. They can also act as the benchmarks for a comparison with the presented comprehensive method.

2.4.1. Collision Speed and Penetration Results under Typical Collision Conditions

Taking the SP1 collision condition as an example, the collision simulation model is shown in Figure 6. Under this collision condition, both the supply ship and the platform are in surge motions. Therefore, the added mass coefficient in surge was selected.

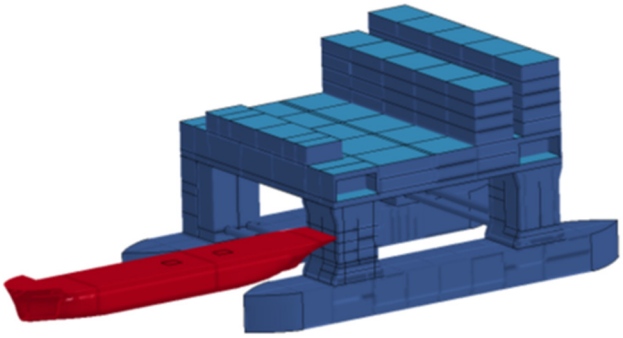

Figure 6. The schematic diagram of the SP1 collision condition.

As shown in Figure 7, after the collision, the ship's speed rapidly decreased to zero at 0.58 s. Then, with the action of the elastic resilience of the platform, the ship's speed started increasing slightly to 0.58 m/s in the negative direction at 0.74 s, and then kept constant, indicating that since 0.74 s, the ship's speed was not affected by other factors. Therefore, the whole collision process lasted for a short period of 0.74 s.

The penetration depth is an essential parameter of collision analysis. The penetration depth can directly reflect the collision intensity and the scale of structural deformation. Figure 8 shows the change in the average penetration with time after the platform pillar collided with the stern of the supply ship. After the penetration depth reached the maximum value of 1.08 m, it declined. At this moment, the residual kinetic energy of the supply ship cannot resist the elastic resilience generated by the deformation of the platform.

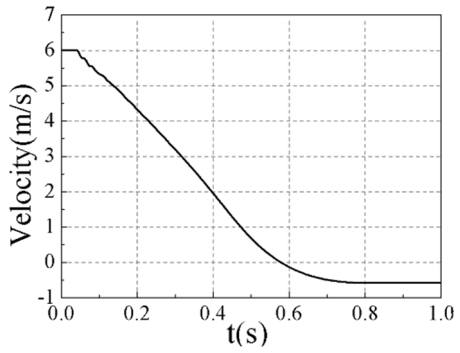

Figure 7. The time-history speed of the ship.

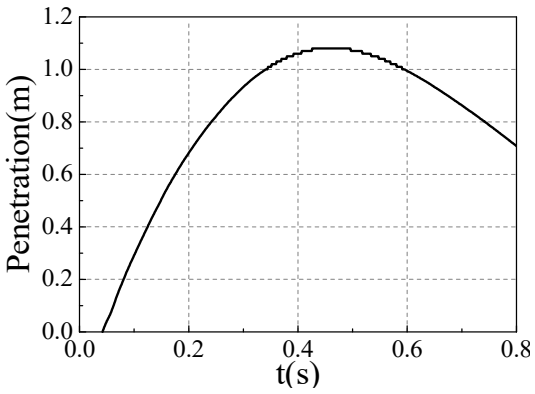

Figure 8. The time-history penetration.

2.4.2. Impact Force Results under Typical Collision Conditions

The collision force reflects the collision intensity between the ship and the support platform, which is the inherent characteristic of the structures. Figure 9 shows a time–history curve of the collision force in the collision condition of SP1. During the entire collision process, due to the local vibration acceleration, the collision force curve appears to oscillates. Its fitting curve is given to show the changing trend of collision force. At the initial impact stage within 0.05 s, the impact force rose rapidly. With the continuous expansion of the deformation range of the pillar components, the induced resistance on the ship stern also increased continuously, and the impact force reached the maximum value of 73.6 MN at about 0.4 s.

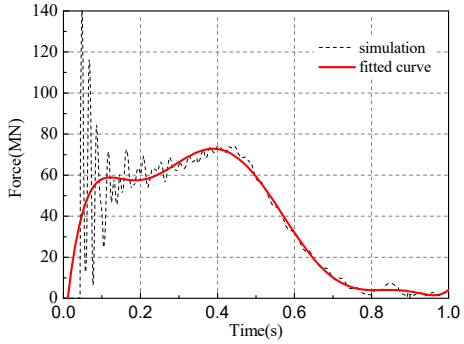

Figure 9. The collision force–time curve.

The force–penetration curve is shown in Figure 10. After the penetration depth reached the maximum value of 1.08 m, the residual kinetic energy of the supply ship was not enough to resist the elastic deformation of the platform, resulting in a rapid decline in the collision force.

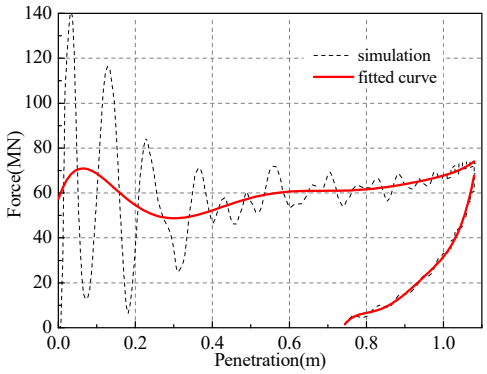

Figure 10. The force–penetration curve.

2.4.3. Energy Conversion Results under Typical Collision Conditions

The energy conversion in the collision process can mainly be described as the initial kinetic energy of the supply ship transformed into the internal energy and kinetic energy of the support platform, the remaining kinetic energy of the supply ship, and the energy loss caused by friction. Generally, the mutual conversion occurs between kinetic energy and internal energy for the whole collision system. The energy conversion in the whole collision system is shown in Figure 11.

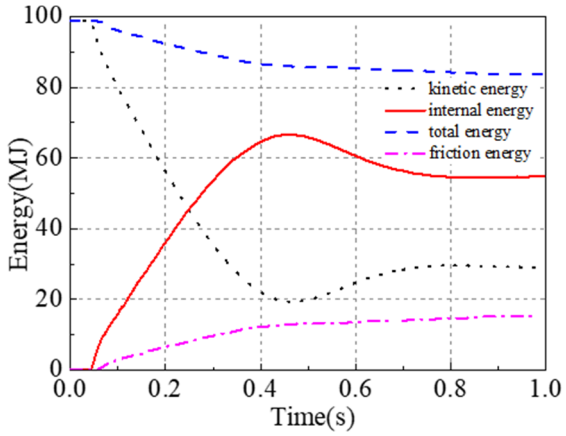

Figure 11. The time–history energy conversion of the collision system.

As seen in Figure 11, the total energy of the system continued to decrease as the collision progressed. Without considering the internal friction of the structure, the total energy loss was caused by external friction. The supply ship energy and platform energy reached the maximum at the same time. Then, the energy changed in a negative direction, which was due to the fact that the structure in the area where the platform collided had both plastic energy absorption and elastic energy absorption, and the release of elastic energy absorption resulted in the conversion of internal energy to kinetic energy. At the end of the collision, the two colliding bodies were separated, and then the energy of each part of the system remained constant.

2.4.4. Comparison of Collision Damage at Different Collision Positions

The stress nephograms in the collision conditions of SP1, SP4, SP5, and SP6 are shown in Figure 12. The comparison showed that the damage and deformation of the column structure under the three collision conditions of both X and Y directions were basically similar, and the main deformation types were stretching, warping, folding, crushing, and bending.

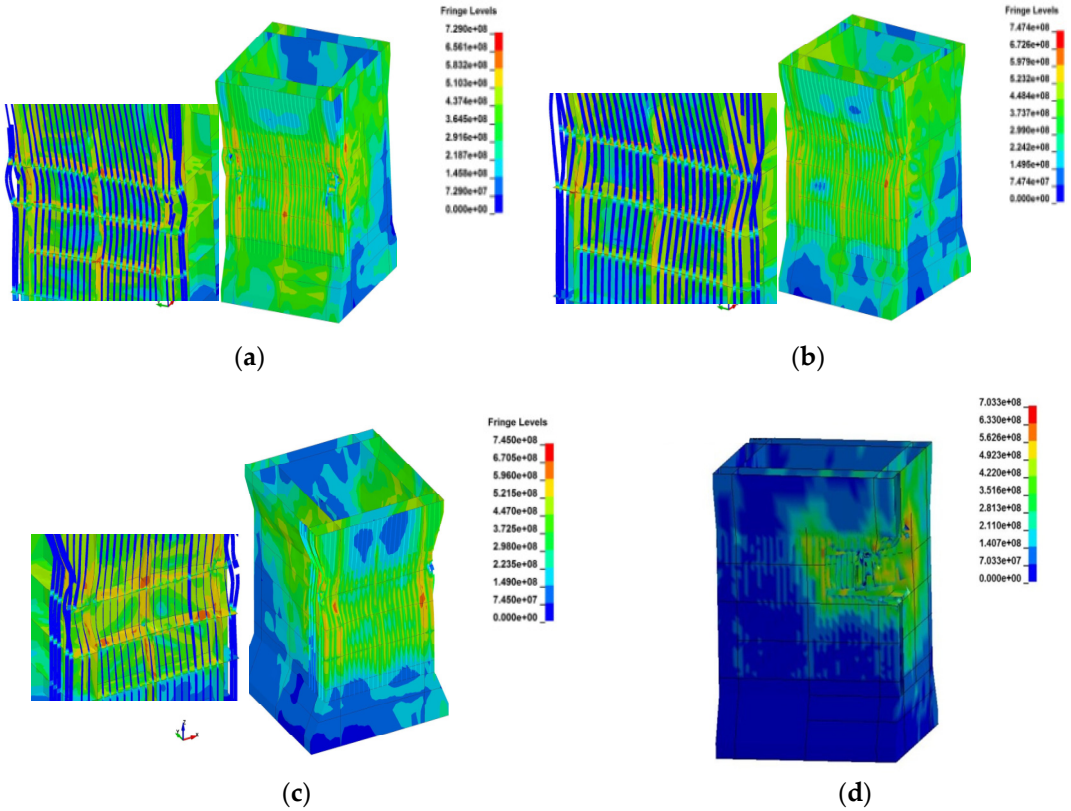

Figure 12. The stress nephograms in different collision areas. (**a**) S-SP1 stress nephogram. (**b**) S-SP4 stress nephogram. (**c**) S-SP5 stress nephogram. (**d**) S-SP6 stress nephogram.

All four collision conditions had an impact velocity of 6 m/s, with a maximum stress of 7.474×10^8 N being generated by the impact of SP4 when the supply ship struck the connection of the horizontal frame of the floating platform in the X-direction. The maximum stress in the case of SP1 was 7.29×10^8 N, slightly less than that in the case of SP4. However, the outer plate of the column of SP1 produced more failure cells and more severe damage than SP4 due to the presence of the horizontal frame, which concentrated the plastic deformation of the outer plate. With different hitting heights, the maximum stress in SP5 was 7.45×10^8 N, slightly smaller than that in SP4. This shows that the collision at the strong frame could lead to less damage on the platform than at the position between the strong frames. In the SP6 condition, the maximum damage to the transition position of the column was more serious than in SP1, SP4, and SP5. Therefore, collisions in the oblique directions should be avoided.

3. Simplified Analysis Method of Collision Process between a Supply Ship and a Semi-Submersible Support Platform

In this section, the external dynamics model proposed by Liu [35] was first applied to simplify the coordinates of the collision between the ship and the offshore platform. Next, dissipated energies under various collision conditions were calculated using external dynamics theory. Then, the deformed energy absorption formula of the structural components of the offshore platform is presented. Through the theoretical analysis via internal dynamics, the energy absorption formulas were reasonably combined according to the specific form of the structure in the collision area. The structure's energy absorption and penetration curves under different collision conditions were obtained. Finally, the critical parameter to measure the collision severity and penetration depth could be calculated. Figure 13 exhibits the detailed analysis process.

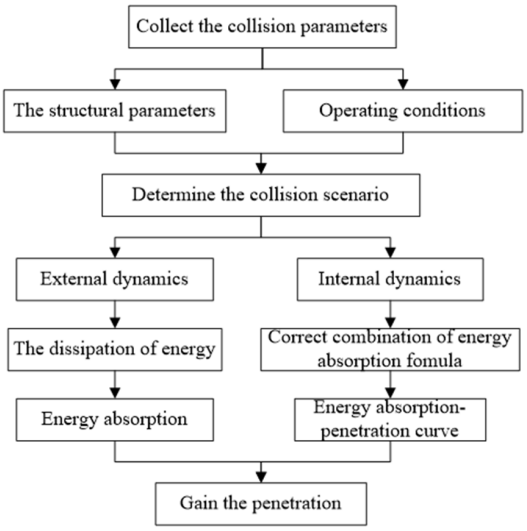

Figure 13. The collision penetration analysis process in the proposed method.

3.1. Theoretical Analysis Based on External Dynamics

In the collision model based on external dynamics [35], some assumptions were made as follows:

(1) The collision process lasts for a very short period, while the collision force is extremely large, and other external forces can be ignored;
(2) Compared with the whole structure, the deformation area caused by collision is small, so the overall geometric configuration between the colliding bodies remains unchanged.

The collision mechanics model [35] is shown in Figure 14.

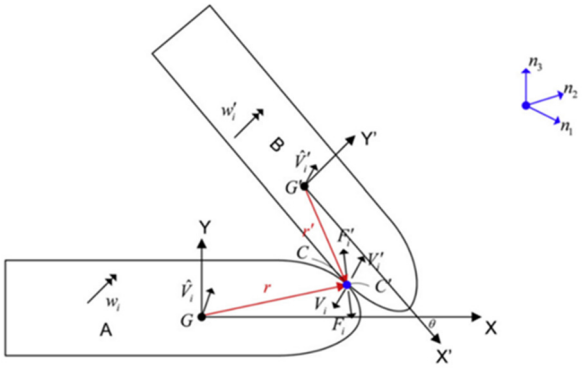

Figure 14. The coordinate system for the collision.

The collision occurred at point C. The collision surface was assumed as a tangential plane through point C, where n_3 represents the normal vector of the section, while n_1 and n_2 are in the section, in which n_1 points to the ship bow, and n_2 represents the normal direction of the plane formed by n_1 and n_3. Two global coordinate systems were established with the center of gravity of each colliding body as the corresponding origin. The local coordinate system was established with collision point C as the origin.

3.1.1. Transformation Matrix and Coordinate Transformation

The general coordinate transformation formula for arbitrary-angle three-dimensional ship–ship collision [35] is introduced as follows. The collision of the supply ship and the offshore platform analyzed in this paper had its own distinctive particularity. The section of the collision system coincided with the collision surface at the stern of the supply ship and the collision surface at the column of the offshore platform. Therefore, the n_1, n_2, and n_3

directions of the local coordinate system can be synchronized to the X, Y, and Z directions of the global coordinate system of the collided platform (see Figure 15).

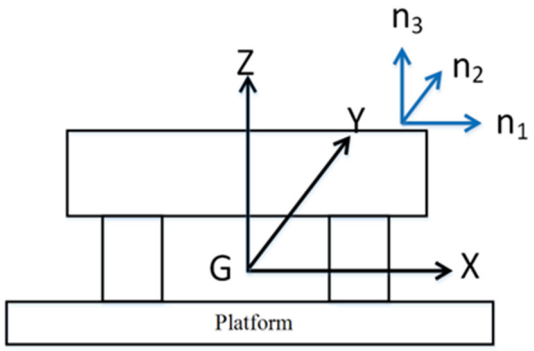

Figure 15. The coordinate system used in this paper.

As the angle of impact is θ, change the global coordinate system of the ship to the local coordinate system, which is also the global coordinate system of the offshore platform. The transformation matrix [15] is displayed as follows:

$$T_{ab} = \begin{bmatrix} cos\theta & -sin\theta & 0 \\ sin\theta & cos\theta & 0 \\ 0 & 0 & 1 \end{bmatrix} \tag{5}$$

When the initial relative velocity is v_i^0, the formulas of the dissipation of energy in three directions [15] are as follows:

$$\begin{aligned} E_1 &= \tfrac{1}{2}\mathrm{abs}\left(\overline{m}_1 \Delta v_1^2\right) = \tfrac{1}{2}\mathrm{abs}\left[\overline{m}_1 \left(e^2 - 1\right)\left(v_1^0\right)^2\right] \\ E_i &= \tfrac{1}{2}\mathrm{abs}\left(\overline{m}_i \Delta v_i^2\right) = \tfrac{1}{2}\mathrm{abs}\left[\overline{m}_i \left(v_i^0\right)^2\right], i = 2,3 \end{aligned} \tag{6}$$

where 'abs' indicates calculating the absolute value and e is the restitution coefficient varying between 0 and 1, which is defined here by the ratio of the normal velocity of the colliding body before and after the collision, as shown in Equation (7). When $e = 0$, there is no rebound, and the two colliding bodies stick together after the collision with the maximum kinetic energy loss; when $e = 1$, it means a complete rebound without kinetic energy loss.

According to the simulation results shown in Table 8, the value of the restitution coefficient is mainly related to the structure involved in the collision, with relatively little relationship with the collision condition. Accordingly, the collision restitution coefficient was uniformly evaluated as 0.45 in this research. This coefficient [15] could be used to calculate the dissipated energy for different collision conditions.

$$e = \left| \frac{v_n(t = T)}{v_n(t = 0)} \right| \tag{7}$$

Table 8. The relative velocity before and after collision under various collision conditions.

Collision Condition	v_n (t = 0) (m/s)	v_n (t = T) (m/s)	Restitution Coefficient e
S-SP1	6	2.57	0.428
S-SP2	2	0.93	0.465
S-SP3	4	1.64	0.410
S-SP4	6	2.71	0.452
S-SP5	6	2.90	0.480
S-SP6	6	2.42	0.400

3.1.2. Results of Dissipated Energy

The calculation results under various collision conditions based on the external dynamics had a deviation less than 5% compared with the obtained numerical simulation results, as shown in Table 9. It implies that the analytical method of the external dynamics theory used in this paper is applicable to the calculation of the dissipated energy of the collision between the 5000 t supply ship and the 33,500 t support platform, and the selected restitution coefficient is relatively accurate. Meanwhile, we can conclude that under the condition of the same impact velocity, the dissipated energy would be almost similar. With increasing collision velocity, the dissipated energy also rises, indicating that the collision velocity is greatly affected in dissipated energy.

Table 9. The dissipated energy comparison between the simulation results and theoretical analysis results.

Collision Condition	Simulated Dissipated (MJ)	Analytical Dissipated (MJ)	Error (%)
S-SP1	70.0	70.4	0.5
S-SP2	7.8	7.8	0
S-SP3	31.8	31.3	1.6
S-SP4	73.6	70.4	4.3
S-SP5	72.4	70.9	2.1
S-SP6	75.6	73.4	2.9

3.2. Theoretical Analysis Based on Internal Dynamics

Before the simplified analysis based on internal dynamics, the collision scene should be defined first, namely, the specific position of the rammed column, the speed, mass, and shape of the ship, the specific components of the structure in the rammed area and their characteristic sizes. Then, the form and quantity of the structural components involved in energy absorption are determined, and proper calculation formulas are determined according to reasonable combinations of various deformation modes. Finally, the curves of the energy absorption and penetration of the platform structure under different collision conditions are drawn to obtain the penetration of the impacted structure.

3.2.1. Basic Assumptions

In the actual collision scene, the dissipated kinetic energy of a collision system is mainly transformed into deformation energy and friction energy. Define C_f as the friction loss energy ratio coefficient, which is defined as friction energy E_f divided by dissipated energy ΔE_k:

$$C_f = \frac{E_f}{\Delta E_k} \tag{8}$$

According to the simulation results of the energy loss shown in Table 10, the friction energy ratio coefficient was found to vary slightly among different conditions. Accordingly, it could be determined as 0.21 when calculating the energy absorption in different collision scenarios.

Table 10. The ratio of the friction energy to dissipated energy.

Collision Condition	Dissipated Energy (MJ)	Friction Energy (MJ)	Coefficient C_f
S-SP1	70.0	13.70	0.196
S-SP2	7.8	1.81	0.232
S-SP3	31.8	6.93	0.218
S-SP4	73.6	13.46	0.183
S-SP5	72.4	15.20	0.210
S-SP6	75.6	16.90	0.224

Then, with the known ΔE_k and C_f, friction energy E_f can be derived. Through the energy conversion process, the total energy absorption can be deducted by the known friction energy and initial kinetic energy.

3.2.2. Deformation Modes of Basic Structural Components in the Offshore Platform

This part provides the relation of the energy absorption and penetration depth. The key point of the internal dynamics analysis is to determine the deformation mode of the structural components. The deformation patterns of the basic structures of the offshore platforms are introduced below.

(1) Shell plate subjected to a lateral area load (suitable for the collision between a ship stern and a plate) [36]

As shown in Figure 16, the plane of the stern was reduced to a rectangular plane with the size of $2a_0 \times 2b_0$ when the stern collided with the platform column. In this case, the impact force F_p and the structural energy absorption E_p were analyzed as follows.

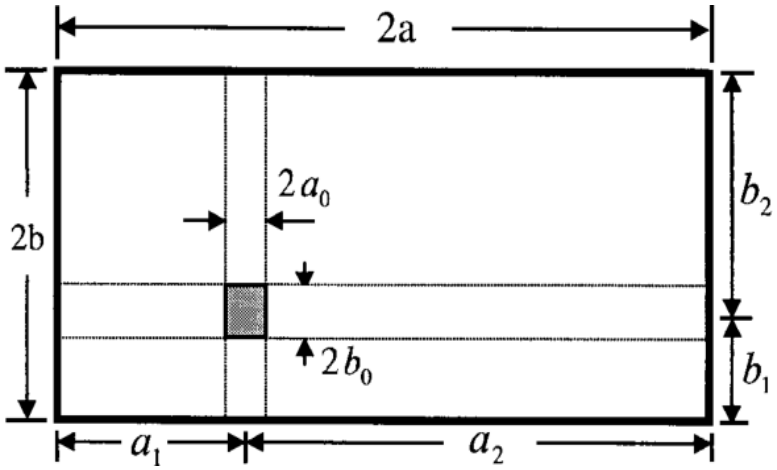

Figure 16. The schematic diagram of the rectangular plate impacted by rectangular load.

When the ship stern collides with the platform column, the plane of the stern is reduced to a rectangular plane with the size of $2a_0 \times 2b_0$. In this case, the relation of impact force F_p and structural energy absorption E_p with penetration depth δ [36] are:

$$F_p = \frac{8}{3\sqrt{3}}\sigma_0 t\delta\left(\frac{b-b_0}{a_2-a_0}+\frac{a-a_0}{a_2-a_0}\right)+\frac{8}{\sqrt{3}}\sigma_0 t\delta\left(\frac{(b-b_0)a_0}{(b-b_0)(b_2-b_0)}+\frac{(a-a_0)b_0}{(a-a_0)(a_2-a_0)}\right) \quad (9)$$

$$E_p = \int_\delta F_p d\delta = \frac{4}{3\sqrt{3}}\sigma_0 t_p\delta^2\left(\frac{b-b_0}{a_2-a_0}+\frac{a-a_0}{a_2-a_0}\right)+\frac{4}{\sqrt{3}}\sigma_0 t_p\delta\left(\frac{(b-b_0)a_0}{(b-b_0)(b_2-b_0)}+\frac{(a-a_0)b_0}{(a-a_0)(a_2-a_0)}\right) \quad (10)$$

where δ means the penetration depth and σ_0 is typically assumed to be constant and taken as the average of the initial yield stress and ultimate stress. The notations are also suitable for Equations (11)–(16).

(2) The vertical compression model of the plate

Generally, the back of an outer plate has a strong rib frame, longitudinal girder, and other structures for the strength enhancement of the plate. The theoretical model presented by Hong [37] is suitable for this kind of collision, and its solution principle is shown in Figure 17. The expressions of collision force and structure energy absorption [37] are:

$$\begin{gathered} F_s = \frac{17M_0(b/t)^{1/3}}{\lambda} \\ M_0 = \sigma_0 \cdot t/4 \end{gathered} \quad (11)$$

$$E_s = \int_H F_s dh = 17M_0\lambda^{-1}(b/t)^{1/3}\delta \quad (12)$$

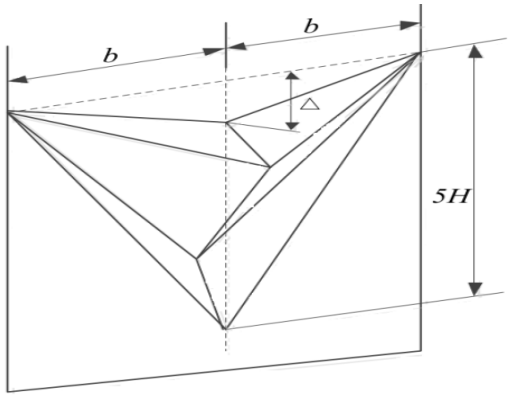

Figure 17. The assumed deformation mode for web crushing.

(3) Collision of web and stringer intersections (T-shaped structure and cross structure)

In this part, a modified model [36] was used to calculate the energy absorption of these two structures under pressure. The model principle is shown in Figure 18. The average collision force F_T, F_X of the two structures and the energy absorption E_T and E_X of the structures [36] are as follows:

$$F_T = 2.8470\sigma_0 t^{1.5} c^{0.5} + 3.036\sigma_0 t^2 \quad c = b + b + b \tag{13}$$

$$F_X = 3.287\sigma_0 t^{1.5} c^{0.5} + 4.048\sigma_0 t^2 \quad c = b + b + b + b \tag{14}$$

$$E_T = \delta F_T \tag{15}$$

$$E_X = \delta F_X \tag{16}$$

where c is the characteristic length of T-shaped plate frame or cross plate frame and b is the side length of the T-shape plate frame or cross plate frame.

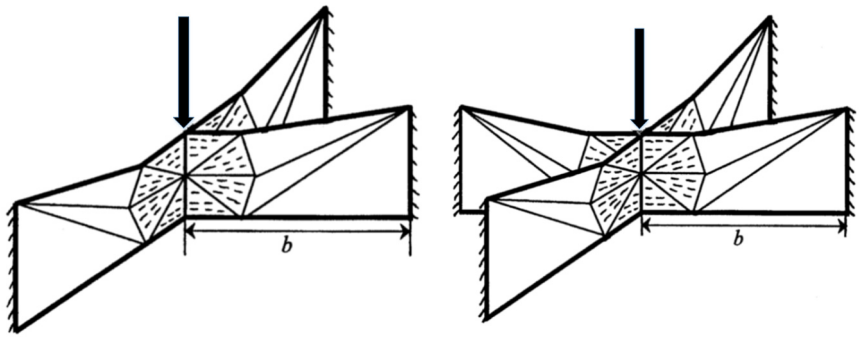

Figure 18. The schematic diagram of the T-shaped frame (**left**) and cross frame (**right**).

3.2.3. Penetration Analysis Based on Internal Dynamics

According to the above-mentioned equations, the curves of the structural energy absorption changing with the penetration depth were obtained by both internal dynamics, as shown in Figure 19. Then, with the known curves and energy absorption, the penetration depths in different conditions could be calculated.

Collision conditions SP1, SP2, and SP3 refer to the rectangular stern colliding with the strong frame of the column, and the energy-absorbing components involved in these impacted areas are the combination of the rectangular plate structure, a cross structure, and two T-shape structures. Collision condition SP4 refers to the rectangular stern colliding with the position between the two strong frames of the column, and the energy absorbing

components involved in the impacted area are the combination of the rectangular plate structure and three stringer structures. Collision condition SP5 refers to the rectangular stern impacting the side of the column, and the energy absorbing structure involved in this collision area is the combination of the rectangular plate structure and two cross structures.

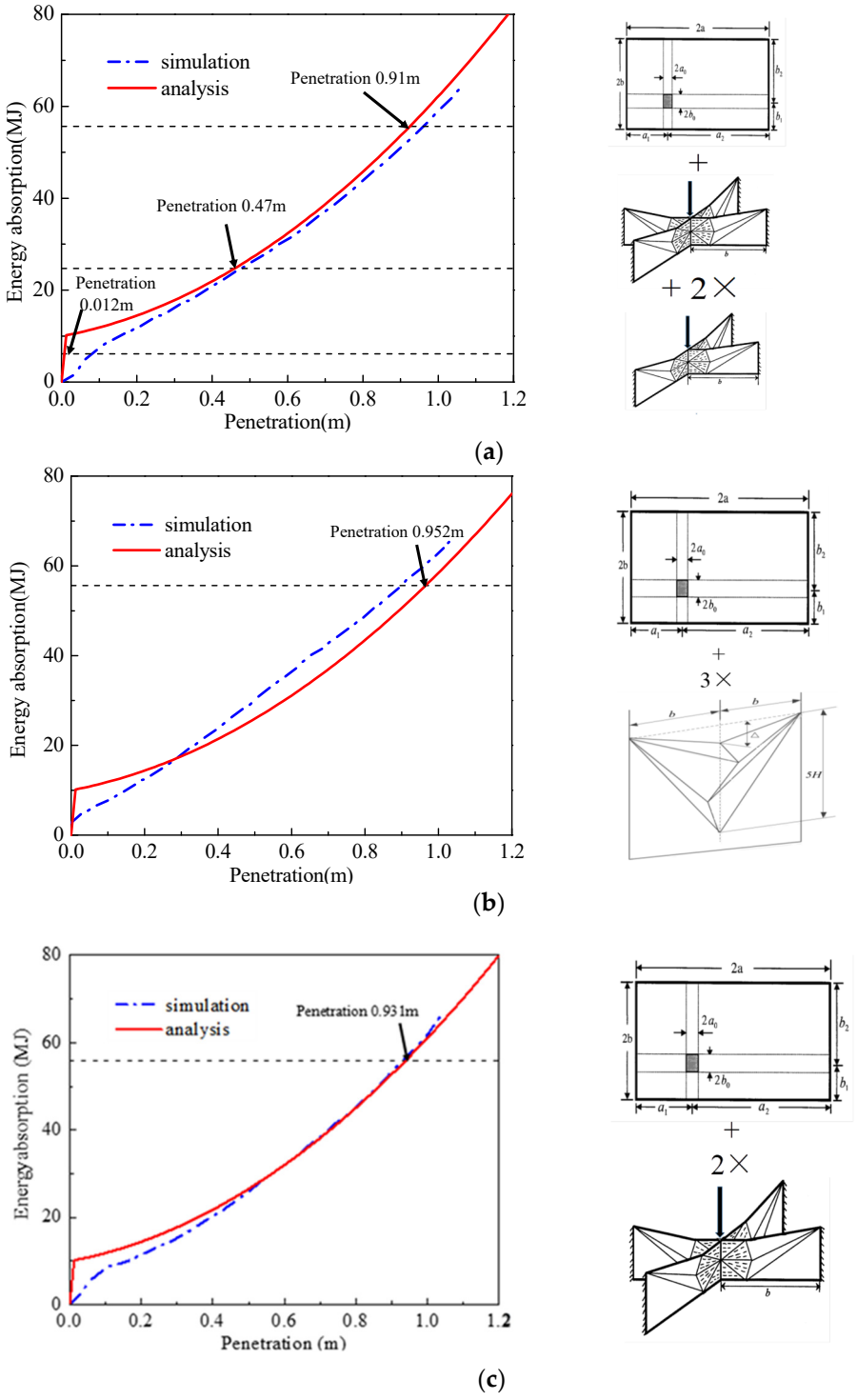

Figure 19. Energy absorption-penetration curves under various collision conditions. (**a**) S-SP1,2,3. (**b**) S-SP4. (**c**) S-SP5.

In the S-SP1,2,3 and S-SP5 conditions, the red curve of the internal dynamics method was higher for lower energy impacts with an energy absorption below 25 MJ compared to

the blue curve of the numerical simulation. Nevertheless, it is in better accordance with the numerical simulation for higher energy impacts above 25 MJ until the penetration depth reached 0.9 m or more. In the S-SP4 case, the internal dynamics approach was about 0.05 m higher for penetration depths for energy absorptions greater than 18 MJ compared to the numerical simulations. Furthermore, the error level was acceptable enough for practical engineering. We concluded that when the penetration depth was below 0.4 m, which is the initial stage of the collision process, the two curves were quite different by the internal dynamics model and simulation. This is because most of the formulas used in the internal dynamics theory are based on the assumption of large deformation plasticity dynamics, so the resulting accuracy is relatively acceptable for extensive deformation conditions. For extremely low energy collisions, elastic energy plays a vital role in the collision process, and the corresponding analytical model is not suitable.

In general, the red curves above were close to the numerical ones for the high-energy collision conditions, which are the potentially hazardous conditions we are concerned with. More importantly, the penetration depths obtained by the proposed simplified method were nearly proven to match the numerical simulation results. It is feasible to assume constant essential parameters for two specific floating bodies and then use the superposition method of failure structures for penetration depth estimation. In summary, the calculation accuracy of the proposed method could reach the level of accuracy of the full numerical simulation method. Due to the simplified algebraic computation, the final result costs significantly decreased with time compared to the numerical simulation when numerous different conditions were considered. This indicates the advantage of the proposed combined method.

The compared penetration depths based on internal dynamics and simulation are displayed in Table 11. It can be seen that under the SP2 collision condition, the deviation was substantial. This is because the initial kinetic energy of the collision system under the SP2 collision condition was small, which belongs to the low-energy collision. In contrast, the deviation of the penetration depth under the other collision conditions was smaller than 15%.

Table 11. The simulation results and analytical results of the penetration depth.

Collision Condition	Simulation (m)	Analytical (m)	Error (%)
S-SP1	1.07	0.910	14.95
S-SP2	0.09	0.012	86.50
S-SP3	0.79	0.470	3.69
S-SP4	1.12	0.952	15.00
S-SP5	0.93	0.931	0.423

Therefore, the presented simplified method could calculate the penetration depth based on two key coefficients obtained by the simulation. For large-energy collisions, the method is acceptable for the preliminary estimation of the penetration depth.

4. Conclusions

This paper presents a simplified method for evaluating the penetration depth in the collision process by combining the external dynamics model, internal dynamics model, and numerical simulation results. A specific collision process between a supply ship and a semi-submersible platform was studied, and different collision speeds, positions, and angles were considered. We improved the corresponding energy absorption formula through the linear combination of different components according to the different hitting areas when using the internal dynamics. Finally, the conclusions were made as follows.

(1) From the simulation results, we concluded that the damage and deformation of the impacted structure appeared to be prominent local characteristics. Under the condition of a specific impact velocity, when the collision area is closer to horizontal strong frames, the damage to the platform will be more serious. This is because

there are more constraints in this position, which leads to more shear failure in the platform structure. Otherwise, the damage to the column is more severe with an oblique impact angle than with a positive angle. Therefore, inclined angle operations should be avoided when the actual supply ship berths to the offshore platform for supply service.

(2) According to the simulation results in different conditions, both the restitution coefficient and friction energy ratio coefficient were deducted. More importantly, the two coefficients were found to vary little from the different collision conditions. This makes the coefficients easily determined by individual representative numerical simulation. Then, the penetration depths can be calculated based on combining these coefficients with the external and internal dynamics models. Compared with the numerical simulation results, the obtained penetration depths showed errors more minor than 15% in medium- to large-energy collision scenarios. This indicates that the presented method is suitable for a fast and initial evaluation of the penetration depths between the ships and offshore platforms.

(3) The restitution coefficient and friction energy ratio may mainly be related to some of the inherent characteristics of collision bodies. Moreover, the coefficients could be determined and adjusted when applied to other floating bodies.

The proposed method is suitable to roughly evaluate the penetration depth in most offshore platforms since it comprises steel frames with horizontal and vertical strong structures. The adaptability and feasibility of the method in different collision conditions are expected to be studied in the future.

Author Contributions: Conceptualization, Y.X. and X.Z.; Methodology, Y.X.; Software, Y.X.; Validation, Y.X., Z.Y. and X.Z.; Data curation, Z.Y.; Writing—original draft preparation, Y.X.; Writing—review and editing, Y.X. and Z.Y.; Project administration, X.Z.; Funding acquisition, X.Z. All authors have read and agreed to the published version of the manuscript.

Funding: The research was funded by the National Natural Science Foundation of China (Grant No. 52001112) and the Fundamental Research Funds for the Central Universities (No. B210202022).

Institutional Review Board Statement: Not applicable.

Informed Consent Statement: Not applicable.

Data Availability Statement: Not applicable.

Conflicts of Interest: The authors declare no conflict of interest.

References

1. Amiri, N.; Shaterabadi, M.; Reza Kashyzadeh, K.; Chizari, M. A Comprehensive Review on Design, Monitoring, and Failure in Fixed Offshore Platforms. *J. Mar. Sci. Eng.* **2021**, *9*, 1349. [CrossRef]
2. Chen, J.; Di, Z.; Shi, J.; Shu, Y.; Zhang, W. Marine Oil Spill Pollution Causes and Governance: A Case Study of Sanchi Tanker Collision and Explosion. *J. Clean. Prod.* **2020**, *273*, 122978. [CrossRef]
3. Wang, Y.-F.; Wang, L.-T.; Jiang, J.-C.; Wang, J.; Yang, Z.-L. Modelling ship collision risk based on the statistical analysis of historical data: A case study in Hong Kong waters. *Ocean Eng.* **2020**, *197*, 106869. [CrossRef]
4. Hanafiah, R.M.; Zainon, N.S.; Karim, N.H.; Abdul Rahman, N.S.F.; Behforouzi, M.; Soltani, H.R. A new evaluation approach to control maritime transportation accidents: A study case at the Straits of Malacca. *Case Stud. Transp. Policy* **2022**, *10*, 751–763. [CrossRef]
5. Ugurlu, H.; Cicek, I. Analysis and assessment of ship collision accidents using Fault Tree and Multiple Correspondence Analysis. *Ocean Eng.* **2022**, *245*, 110514. [CrossRef]
6. Zhang, M.; Zhang, D.; Goerlandt, F.; Yan, X.; Kujala, P. Use of HFACS and fault tree model for collision risk factors analysis of icebreaker assistance in ice-covered waters. *Saf. Sci.* **2019**, *111*, 128–143. [CrossRef]
7. Martins, M.R.; Maturana, M.C. Human Error Contribution in Collision and Grounding of Oil Tankers. *Risk Anal.* **2010**, *30*, 674–698. [CrossRef]
8. Ramos, M.A.; Thieme, C.A.; Utne, I.B.; Mosleh, A. Human-system concurrent task analysis for maritime autonomous surface ship operation and safety. *Reliab. Eng. Syst. Saf.* **2020**, *195*, 106697. [CrossRef]
9. Zhang, M.; Conti, F.; Le Sourne, H.; Vassalos, D.; Kujala, P.; Lindroth, D.; Hirdaris, S. A method for the direct assessment of ship collision damage and flooding risk in real conditions. *Ocean Eng.* **2021**, *237*, 109605. [CrossRef]

10. Minorsky, V.U. *An Analysis of Ship Collisions with Reference to Protection of Nuclear Power Plants*; Sharp (George G.) Inc.: New York, NY, USA, 1958; Volume 3.
11. Petersen, M.J. Dynamics of ship collisions. *Ocean Eng.* **1982**, *9*, 295–329. [CrossRef]
12. Pedersen, P.T.; Zhang, S. On Impact mechanics in ship collisions. *Mar. Struct.* **1998**, *11*, 429–449. [CrossRef]
13. Brown, A.J. Collision scenarios and probabilistic collision damage. *Mar. Struct.* **2002**, *15*, 335–364. [CrossRef]
14. Tabri, K.; Broekhuijsen, J.; Matusiak, J.; Varsta, P. Analytical modelling of ship collision based on full-scale experiments. *Mar. Struct.* **2009**, *22*, 42–61. [CrossRef]
15. Liu, Z.; Amdahl, J. On multi-planar impact mechanics in ship collisions. *Mar. Struct.* **2019**, *63*, 364–383. [CrossRef]
16. Zhang, S.; Villavicencio, R.; Zhu, L.; Pedersen, P.T. Impact mechanics of ship collisions and validations with experimental results. *Mar. Struct.* **2017**, *52*, 69–81. [CrossRef]
17. Naar, H.; Kujala, P.; Bo, C.S.; Ludolphy, H. Comparison of the crashworthiness of various bottom and side structures. *Mar. Struct.* **2002**, *15*, 443–460. [CrossRef]
18. Ehlers, S.; Broekhuijsen, J.; Alsos, H.S.; Biehl, F.; Tabri, K. Simulating the collision response of ship side structures: A failure criteria benchmark study. *Int. Shipbuild. Prog.* **2008**, *55*, 127–144.
19. Dekker, R.; Walters, C.L. A global FE–local analytical approach to modelling failure in localised buckles caused by crash. *Ships Offshore Struct.* **2017**, *12*, S1–S10. [CrossRef]
20. Haris, S.; Amdahl, J. An analytical model to assess a ship side during a collision. *Ships Offshore Struct.* **2012**, *7*, 431–448. [CrossRef]
21. Sun, B.; Hu, Z.; Wang, G. An analytical method for predicting the ship side structure response in raked bow collisions. *Mar. Struct.* **2015**, *41*, 288–311. [CrossRef]
22. Liu, B. Analytical method to assess double-hull ship structures subjected to bulbous bow collision. *Ocean Eng.* **2017**, *142*, 27–38. [CrossRef]
23. Liu, B.; Soares, C.G. Analytical method to determine the crushing behaviour of girders with stiffened web. *Int. J. Impact Eng.* **2016**, *93*, 49–61. [CrossRef]
24. Liu, B.; Villavicencio, R.; Zhang, S.; Guedes Soares, C. Assessment of external dynamics and internal mechanics in ship collisions. *Ocean Eng.* **2017**, *141*, 326–336. [CrossRef]
25. Pill, I.; Tabri, K. Finite element simulations of ship collisions: A coupled approach to external dynamics and inner mechanics. *Ships Offshore Struct.* **2011**, *6*, 59–66. [CrossRef]
26. Liu, Z. Numerical simulation of dropped container impacts with an offshore platform deck in the North Sea. *Proc. Inst. Mech. Eng. Part M J. Eng. Marit. Environ.* **2021**, *236*, 273–282. [CrossRef]
27. Column-Stabilised Units. In *DNV-RP-C103*; Det Norske Veritas: Bærum, Norway, 2015. Available online: https://rules.dnv.com/docs/pdf/DNV/RP/2021-10/DNV-RP-C103.pdf (accessed on 30 April 2022).
28. Structural Design against Accidental Loads. In *DNV-RP-C204*; Det Norske Veritas: Bærum, Norway, 2019. Available online: https://www.dnv.com/oilgas/download/dnv-rp-c204-structural-design-against-accidental-loads.html (accessed on 30 April 2022).
29. Paik, J.K.; Chung, J.Y.; Chun, M.S. On Quasi-Static Crushing of a Stiffened Square Tube. *J. Soc. Nav. Archit. Korea* **1996**, *33*, 109–123. [CrossRef]
30. Korgesaar, M.; Romanoff, J. Influence of mesh size, stress triaxiality and damage induced softening on ductile fracture of large-scale shell structures. *Mar. Struct.* **2014**, *38*, 1–17. [CrossRef]
31. Jones, N. *Structure Impact*; Cambridge University Press: Cambridge, UK, 1989.
32. March, P.I. LS-DYNA Manual R 11.0—Vol I: California, USA. 2018. Available online: https://www.dynasupport.com/manuals/ls-dyna-manuals/ls-dyna-manuals/ls-dyna_manual_volume_i_r11.pdf/view (accessed on 30 April 2022).
33. Ko, Y.G.; Kim, S.J.; Sohn, J.M.; Paik, J.K. A practical method to determine the dynamic fracture strain for the nonlinear finite element analysis of structural crashworthiness in ship–ship collisions. *Ships Offshore Struct.* **2018**, *13*, 1–11. [CrossRef]
34. Kitamura, O. FEM approach to the simulation of collision and grounding damage. *Mar. Struct.* **2002**, *15*, 403–428. [CrossRef]
35. Liu, Z.; Amdahl, J. A new formulation of the impact mechanics of ship collisions and its application to a ship–iceberg collision. *Mar. Struct.* **2010**, *23*, 360–384. [CrossRef]
36. Zhang, S. The Mechanics of Ship Collisions. Ph.D. Thesis, Technical University of Denmark, Kongens Lyngby, Denmark, 1999.
37. Hong, L. Simplified Analysis and Design of Ships Subjected to Collision and Grounding. Ph.D. Thesis, Norwegian University of Science and Technology, Trondheim, Norway, 2009.